THE JOURNAL OF PHYSICAL CHEMISTRY C

Article

Functionalization of Halloysite Clay Nanotubes by Grafting with #-Aminopropyltriethoxysilane

Peng Yuan, Peter D. Southon, Zongwen Liu, Malcolm E. R. Green, James M. Hook, Sarah J. Antill, and Cameron J. Kepert

J. Phys. Chem. C, **2008**, 112 (40), 15742-15751 • DOI: 10.1021/jp805657t • Publication Date (Web): 12 September 2008

Functionalization of Halloysite Clay Nanotubes by Grafting with γ-Aminopropyltriethoxysilane

Peng Yuan,[†,‡] Peter D. Southon,[‡] Zongwen Liu,[§] Malcolm E. R. Green,[‡] James M. Hook,[||] Sarah J. Antill,[‡] and Cameron J. Kepert*[,‡]

Guangzhou Institute of Geochemistry, Chinese Academy of Sciences, Guangzhou 510640, China, School of Chemistry, The University of Sydney, New South Wales 2006, Australia, Australian Key Centre for Microscopy and Microanalysis, The University of Sydney, New South Wales 2006, Australia, and School of Chemistry, The University of New South Wales, Sydney, New South Wales 2052, Australia

Received: June 27, 2008; Revised Manuscript Received: August 8, 2008

Surface modification of natural halloysite clay nanotubes with γ-aminopropyltriethoxysilane (APTES) was investigated. Untreated and modified samples were characterized by nitrogen adsorption, X-ray diffraction, elemental analysis, thermogravimetry, transmission electron microscopy, atomic force microscopy, MAS nuclear magnetic resonance (^{29}Si, ^{13}C, ^{29}Al), and Fourier transform infrared spectroscopy. The modification mechanism was found to include not only the direct grafting of APTES onto the hydroxyl groups of the internal walls, edges and external surfaces of the nanotubes but other processes in which oligomerized APTES condensed with the directly grafted APTES to form a cross-linked structure. The thermal and evacuation pretreatment conditions were found to play an important role in controlling the extent and mechanism of the modification. The extent of modification is also strongly affected by the morphological parameters of the original clay samples. This study demonstrates that the surface chemistry of halloysite nanotubes is readily modified, enabling applications in nanocomposites, enzyme immobilization and controlled release.

1. Introduction

The modification of oxide surfaces by coupling with functionalized organosilanes is applicable to the fields of catalysis, adsorption, electrochemistry, chromatography and nanocomposite materials. Of particular interest is the use of ordered mesoporous silica materials such as SBA-15[1] and MCM-41[2] as supports for enzyme immobilization, heavy metal adsorption, and heterogeneous catalysis.[3] The mechanisms and applications of the interaction between organosilanes and mesoporous materials have been widely discussed and reviewed.[4−6]

In recent years, the functionalization of clay minerals with organosilane has attracted considerable interest, due mainly to the increasing requirements from the area of polymer-clay nanocomposites.[7] Functionalization of clays with organosilanes has been explored as a way to improve clay dispersal in a polymer matrix, thus increasing the mechanical properties of resultant polymer-clay nanocomposites. Further, the binding properties of organosilane-functionalized clays have been investigated for the treatment of heavy metal contaminants.[8,9] The clay minerals investigated are principally lamellar clays, most notably laponite,[10,11] smectite,[12] kaolinite,[13,14] and montmorillonite,[15,16] and include also the tubular aluminosilicate clay, imogolite.[17]

In the present study, organosilane functionalization of another tubular clay material, halloysite ($Al_2(OH)_4Si_2O_5 \cdot 2H_2O$), was investigated. As a naturally occurring hydrated polymorph of kaolinite, halloysite has a similar structure and composition, but the unit layers are separated by a monolayer of water molecules.[18] As a result, hydrated halloysite has a basal spacing (d_{001}) of 10 Å, which is ∼3 Å larger than that of kaolinite. The interlayer water is weakly held, so that halloysite-(10 Å) can readily transform to halloysite-(7 Å) (also known as metahalloysite) by dehydration.[19,20] Tubular halloysite has a highly unusual meso/macroscopic superstructure, which results from the wrapping of the clay layers around onto themselves to form hollow cylinders under favorable geological conditions. This wrapping process is driven by a mismatch in the periodicity between the oxygen sharing tetrahedral SiO_4 sheets and adjacent octahedral $A1O_6$ sheets in the 1:1 layer.[21−24] In each halloysite nanotube (HNT), the external surface is composed of siloxane (Si−O−Si) groups, whereas the internal surface consists of a gibbsite-like array of aluminol (Al-OH) groups. The schematic representations[21] of the crystalline structure of halloysite-(10 Å) and the structure of a single tubular halloysite particle is shown in Figure 1.

In contrast to kaolinite, very little is known of the chemical and physical properties of halloysite, and there are few applications that aim to utilize the beautiful hollow tubular structure of this mineral. This is despite considerable interest in a range of other synthetic nanotubular solids such as carbon nanotubes (CNTs), and despite the existence of significant deposits in Australia, China, Guyana, Mexico and Brazil.[20]

Generally, the length of halloysite nanotubes varies from ca. 0.02 to 30 μm[20] and the external diameter from ca. 30 to 190 nm, with an internal diameter range of ca. 10−100 nm.[21,25] These dimensions differ considerably from those of imogolite (0.25−0.35 μm in length and ∼0.82 nm in internal diameter). The very large diameter of the halloysite lumen makes it potentially suitable for the accommodation of a range of guests. For instance, halloysite has been shown to be capable of entrapping and subsequently releasing small pharmaceutical

* To whom correspondence should be addressed. Phone: +61 2 9351 5741. Fax: +61 2 9351 3329. E-mail: c.kepert@chem.usyd.edu.au.
† Chinese Academy of Sciences.
‡ School of Chemistry, The University of Sydney.
§ Australian Key Centre for Microscopy and Microanalysis, The University of Sydney.
|| The University of New South Wales.

10.1021/jp805657t CCC: $40.75
Published on Web 09/12/2008

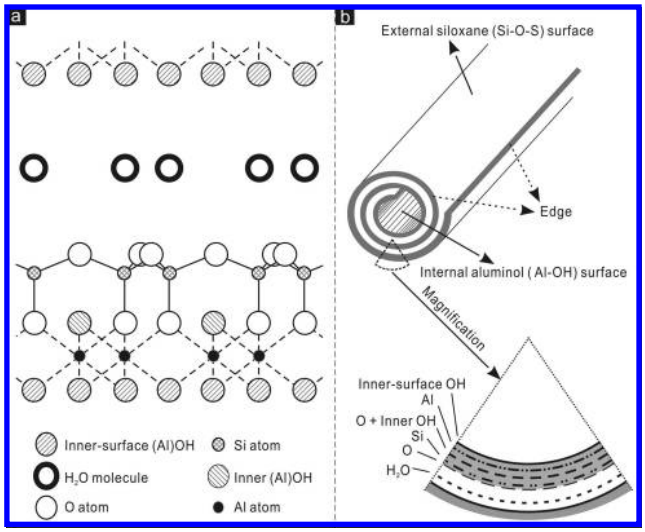

Figure 1. Schematic diagrams of (a) the crystalline structure of halloysite-(10 Å), and (b) the structure of a halloysite nanotube.

molecules.[26,27] In recent reports, the mesoporous lumen of halloysite nanotubes was also used as a nanoreactor to host reactants for nanosynthesis and biomimetic synthesis.[28,29]

Further applications can be postulated. The size of the lumen enables halloysite to be a potential candidate for immobilization of large-sized enzymes, e.g., serum albumin and conalbumin, which even SBA-15 may not be able to host.[30] Furthermore, due to their high surface area, large aspect ratio and hollow structure, halloysite nanotubes could also be combined with a polymer matrix to form low-density nanocomposites, replacing larger quantities of macro- or microcounterparts such as glass or carbon fibers.

Application of halloysite in the above areas is currently severely limited by its highly hydrophillic internal and external surfaces, making surface modification of this clay of urgent interest. Grafting of organosilanes on the internal surface and edges/defects promises to be a particularly versatile yet site-specific approach to surface modification, and one that, to our knowledge, has not yet been explored.

In this work, the surface modification of halloysite by grafting (3-aminopropyl)triethoxysilane (APTES, $H_2NCH_2CH_2CH_2Si(OCH_2CH_3)_3$) was investigated. The objective of this study was to determine how APTES reacts with the surface groups of halloysite, and to explore the influence of pretreatment conditions and halloysite morphology on the reaction mechanism.

2. Experimental Methods

2.1. Materials and Methods. Three raw halloysite samples, PATCH, CLA, and HG, were used for the APTES modification. They were collected from Kalgoorlie in Western Australia, Camel Lake in South Australia, and Northland in New Zealand, respectively. A kaolinite sample from Maoming deposit in China was also used for comparison purposes. All of the raw clay samples were purified by repeated sedimentation processes to remove the quartz impurities, followed by drying at 110 °C for 12 h and grinding. The resultant samples are here referred to as PATCH-110, CLA-110, HG-110, and Kaolinite-110. These halloysite samples were further pretreated to make their derivatives. For example, CLA-400 corresponds to the sample derived from CLA-110 pretreated at 400 °C for 12 h in a muffle oven, and CLA-H is denoted as the rehydrated sample obtained by leaving a portion of CLA-110 in ambient condition for 48 h.

TABLE 1: Pretreatment Conditions and the Names of the APTES-Modified Halloysite Samples

sample	thermal pretreatment	evacuation pretreatment
CLA-H-M	ambient rehydration	none
CLA-H-EM	ambient rehydration	yes
CLA-110-M	110 °C, 12 h	none
CLA-110-EM	110 °C, 12 h	yes
CLA-400-M	400 °C, 12 h	none
CLA-400-EM	400 °C, 12 h	yes
PATCH-110-M	110 °C, 12 h	none
HG-110-M	110 °C, 12 h	none
Kaolinite-110-M	110 °C, 12 h	none

Organosilane modified samples were prepared according to the procedure generally applied for the grafting of silica-based materials.[31] In a typical run, 2 mL of APTES was dissolved in 25 mL of dry toluene. Approximately 0.6 g of clay powder was added, and the suspension was dispersed ultrasonically for 30 min. Evacuation pretreatment (see below) may be carried out at this stage. The suspension was then refluxed at 120 °C for 20 h under constant stirring. In the refluxing system, a calcium chloride drying tube was attached to the end to ensure a dry environment. The solid phase in the resultant mixture was filtered and extensively washed six times with fresh toluene to remove the excess organosilane, then dried overnight at 120 °C for further curing. APTES (99%, Aldrich) was used as received. Toluene (AR grade, Aldrich) was used after distillation over activated molecular sieves.

An evacuation pretreatment was applied, designed to remove air from the lumen and promote APTES loading, based on a procedure used to load the drug diltiazem HCl into the lumen of halloysite nanotube.[27] The flask containing the ultrasonically dispersed mixture was evacuated using a vacuum pump, and a slight fizzing of the suspension was observed as the air was removed. After the fizzing stopped, the flask was sealed for 30 min to reach equilibrium and the evacuation process repeated twice. The evacuated suspension was then transferred to the refluxing system for modification.

The sample-specific pretreatment conditions and names for the modified halloysite samples are summarized in Table 1. The APTES-modified samples are differentiated by the suffix -M or -EM, corresponding to nonevacuated or evacuation pretreated samples, respectively.

2.2. Characterization methods. A Shimadzu S-6000 X-ray diffractometer equipped with Cu Kα ($\lambda = 0.154$ nm) was used to acquire the XRD patterns of powdered samples. N_2 adsorption−desorption isotherms were measured on a Micromeritics ASAP2020 system at liquid nitrogen temperature. APTES-modified samples were outgassed at 110 °C for 8 h before measurement. Isotherms for unmodified clay samples were measured after outgassing at 110 and 350 °C for 8 h, but no obvious difference between the two results were observed; only the data corresponding to 110 °C outgassing are presented in this paper. The specific surface area of the sample, S_{BET}, was calculated using the multiple-point Brunauer−Emmett−Teller (BET) method.[32] The Barrett−Joyner−Halenda (BJH) method[33] was used to calculate the total volume of pores (2 - 300 nm), V_{pore} and the pore diameter distribution curve. For halloysite samples these distributions had a peak corresponding to the lumen diameter, reported as d_{peak}.

The CHN elemental analyses were performed at the Campbell Microanalytical Laboratory in New Zealand. The content of loaded APTES, M (wt %), was calculated from the content of nitrogen by the equation of $M = M_N \cdot EMW/14$, with the assumption that APTES molecules were completely hydrolyzed

and condensed, where M_N is the content (wt %) of nitrogen obtained by CHN analysis in which the content of nitrogen in original halloysite sample had been subtracted, and *EMW* is the effective molar mass of hydrolyzed and grafted APTES (122 g/mol).

Thermogravimetric analyses (TG) were performed on a TA 2950 TGA HR instruments. Approximately 10 mg of finely ground samples were heated in a platinum crucible with a heating rate of 5 °C/min, under an atmosphere of high purity N_2.

FTIR spectra of the samples were recorded on a Shimadzu 8400 FTIR spectrometer. Specimens for measurement were prepared by mixing 0.9 mg of the sample powder with 70 mg of KBr and pressing the mixture into a pellet. Over 32 scans were collected for each measurement at a resolution of 2 cm^{-1}.

Solid-state NMR spectra were acquired using a Varian Inova-300 spectrometer operating at 75.4 MHz for ^{13}C and 59.4 MHz for ^{29}Si with Chemagnetics 4 and 7.5 mm double air-bearing cross-polarization (CP) probes. Quantities of ca. 100 and 300 mg of the mineral samples were packed into the 4 mm OD rotors and 7.5 mm OD rotors, respectively, and subjected to "magic-angle spinning" (MAS) at various speeds noted below. Spectra were recorded at 21 °C using the following conditions for each nucleus. ^{13}C: 7.5 mm 4 kHz, CPMAS; 4.5 μs, 90° pulse; 1.5 ms contact time; 5 s relaxation delay. ^{29}Si: 4 mm; 3.5 kHz, CPMAS; 5.5 μs, 90° pulse; 2 ms contact time; 3 s relaxation delay. From 100 to 2000 scans were collected for sufficient signal/noise. The secondary references and samples used for Hartman-Hahn match were hexamethylbenzene for ^{13}C (δ_C 17.3 ppm for CH_3 peak); Kaolinite for ^{29}Si ($\delta_{Si} = -91.5$ ppm).[34]

TEM images were obtained with a Philips CM120 electron microscope operating at an acceleration voltage of 120 kV. The specimens were prepared by the following procedure: the clay sample was ultrasonically dispersed in ethanol for 5 min, and then a drop of sample suspension was dropped onto a carbon-coated copper grid, which was left to stand for 10 min before transferred into the microscope.

AFM measurements were carried out under ambient conditions using a Molecular Imaging PicoPlus system equipped with a 8-μm Multipurpose small scanner LCL. The samples were dispersed on a piece of freshly cleaved mica and images were collected under contact mode using a soft cantilever (NP-S20, Veeco, force constant ca. 0.1 nN/nm).

3. Results and Discussion

3.1. Structural and Morphological Characterization. The XRD patterns of the three original halloysite samples, shown in Figure 2a−c, are in good agreement with a previously published pattern for halloysite.[35] CLA-110 consists of single mineralogical phase of halloysite, whereas HG-110 contains very fine particles of quartz and feldspar impurities (<5 wt %) retained in the sedimentation process. A small quantity of illite or montmorillonite clay impurities, indicated by the basal spacing of 1.61 nm, was found in PATCH-110. The kaolinite sample was pure and ordered, as revealed by the XRD pattern (Figure 2d).

CLA-110 and HG-110 exhibit (001) diffraction peaks at ca. 12.3° in 2θ, corresponding to a basal spacing of 0.72 nm, which identifies these samples as halloysite-(7 Å). PATCH-110 is a halloysite-(7 Å) with higher hydration state, revealed by its basal spacing of 0.79 nm. It also contains a small quantity of halloysite-(10 Å), corresponding to the (001) diffraction with basal spacing of 1.05 nm.

The diffraction patterns in Figure 2e−h show that the interlayer distances of APTES-modified clay samples remained

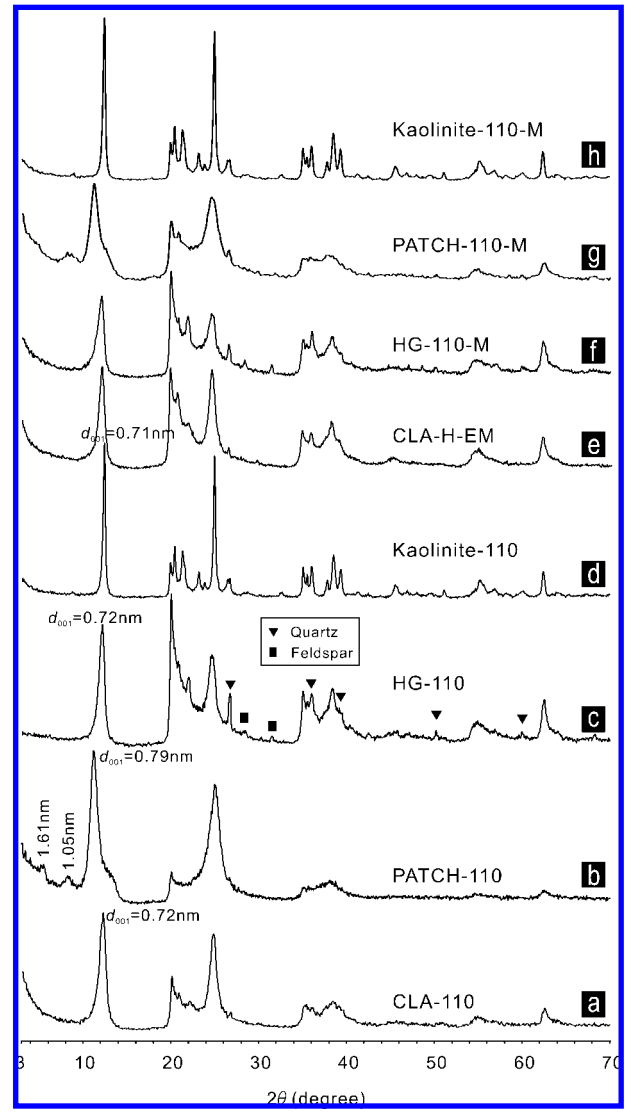

Figure 2. XRD patterns of clay samples.

unchanged, indicating that intercalation of APTES into the interlayer of halloysite or kaolinite did not occur. This result indicates that most of the interlayer inner-surface AlOH groups of both halloysite and kaolinite (Figure 1) were unavailable for grafting, since they were blocked by the strong hydrogen bonds between layers. In previous reports, intercalation with molecules such as dimethyl sulfoxide (DMSO) or *N*-methylformamide[13,36] was proposed as a way to overcome the enthalpic barrier associated with interlayer hydrogen bond breakage. With the DMSO-intercalated clay precursors, various guests such as organosilane,[37] alkanols, diols,[38,39] and methanol,[14] could be introduced into the interlayer of kaolinite to make interlayer-grafted organic derivatives. In this work no preintercalation process was applied, and consequently APTES was not intercalated into the interlayer of halloysite.

The TEM images presented in Figure 3a−c show that the halloysite particles have a cylindrical shape and contain a transparent central area that runs longitudinally along the cylinder, indicating that the nanotubular particles are hollow and open-ended. Among the three halloysite samples, PATCH is thin-walled and highly uniform in length, diameter and morphology, CLA is thick-walled and shows relatively uniform morphology with good tubule quality, and HG has a low tubular quality, characteristic of high irregularity in diameter, wall

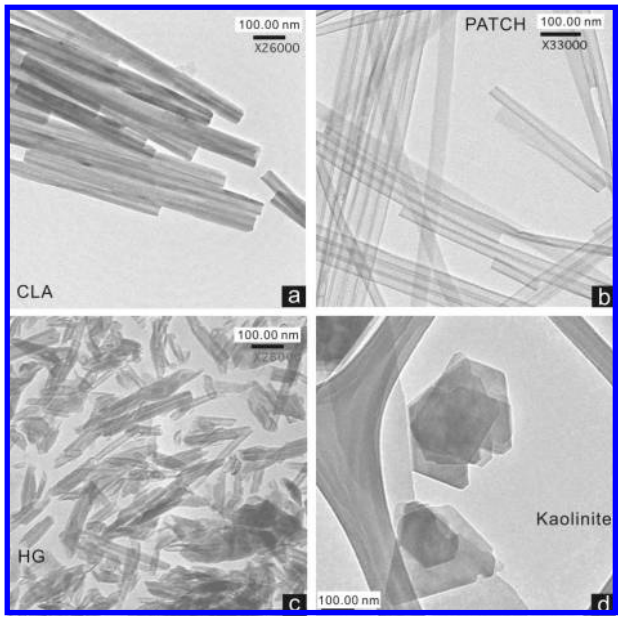

Figure 3. TEM images of (a) CLA, (b) PATCH, (c) HG, and (d) kaolinite.

TABLE 2: Structural Data for Halloysite Samples from TEM and N_2 Adsorption

	CLA-110	PATCH-110	HG-110	Kaolinite-110
L (nm)[a]	850 ± 50	4000 ± 500	200 ± 100	—
D (nm)[b]	52 ± 12	36 ± 3	34 ± 15	—
d (nm)[c]	20 ± 3	19 ± 2	17 ± 9	—
R[d]	~16	~1100	~6	—
T (nm)[e]	18 ± 3	8 ± 3	12 ± 6	—
S_{BET} (m^2/g)	49.5	40.3	23.2	11.8
V_{pore} (cm^3/g)	0.25	0.08	0.13	0.09
d_{peak} (nm)	11.2	7.5	12.1	—

[a] L, the typical length of halloysite particle. [b] D, the typical external diameter. [c] d, the typical internal diameter. [d] R, the aspect ratio, where $R = L/D$. [e] T, the wall thickness of halloysite particle. The values of L, D, d, R, and T are evaluated from TEM images.

thickness and morphology. The morphological parameters of the halloysite samples, measured from the TEM images, are summarized in Table 2. Note that the accuracy of these dimensions is limited by the number of particles observed in the TEM images. Porosity data calculated from the N_2 desorption isotherms, which are of more statistical significance, are given below.

Figure 4 presents some details of surface morphology of the halloysite nanotubes, revealed by combined observation of TEM and AFM. It can seen that some halloysite particles show a concentric structure, of which tubular subunits are concentrically arranged in a telescope-like form (Figure 4a−b). Meanwhile, the lengthways edge of halloysite is well resolved, providing a direct illustration of the curling structure (Figure 4b). Moreover, defects on the surface of halloysite such as surface breakage, probably resulting from mechanical damage (Figure 4a) or crystallographic defects (Figure 4c), are clearly evident. The observation of these morphological details is of great relevance to the surface chemistry of halloysite nanotubes, as it suggests that there exist more surface hydroxyl groups than generally supposed. These extra hydroxyl groups are potential reaction sites for surface modification on the external surface, and should not be overlooked.

The kaolinite sample is composed of plate-like, euhedral particles with typical pseudohexagonal morphology (Figure 3d).

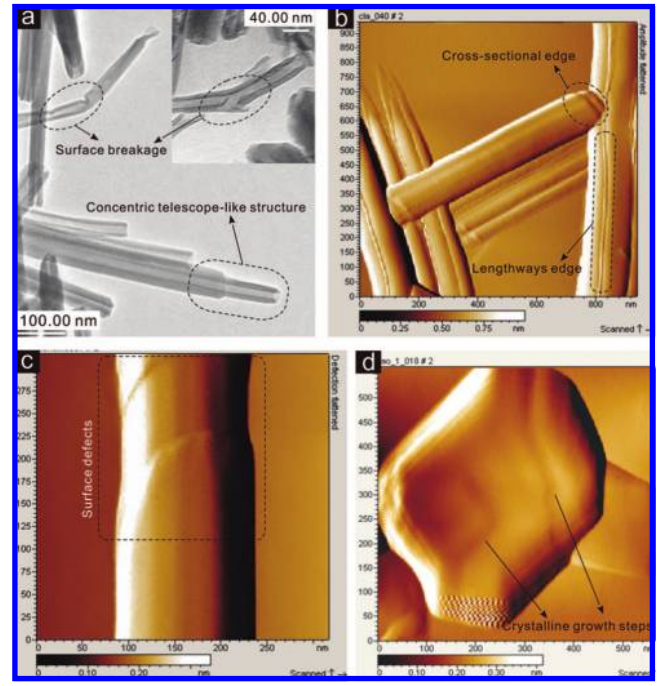

Figure 4. Surface morphological details of sample CLA and kaolinite.

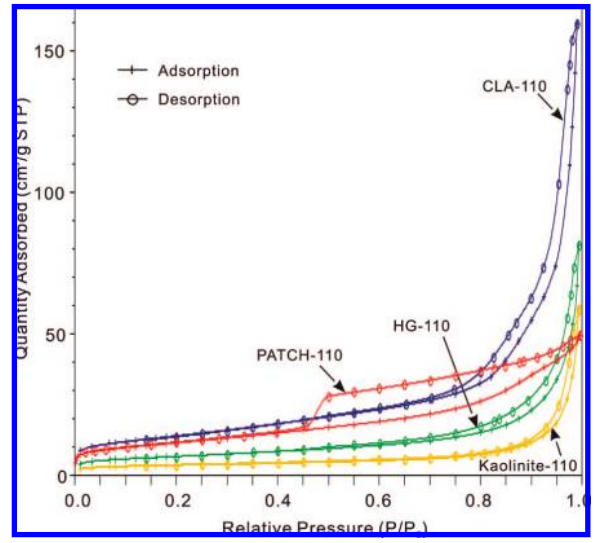

Figure 5. Nitrogen adsorption isotherms of unmodified clay samples.

Simplified as a square particle, kaolinite has a size of about 500 × 500 ± 200 nm, and a particle thickness of ca. 400 ± 150 nm, determined by TEM and AFM. The AFM images (Figure 4d) also reveal the existence of surface defects, such as growing steps, on the kaolinite surface.

The nitrogen adsorption−desorption isotherms of clay samples are depicted in Figure 5. The isotherms of CLA-110, HG-110 and kaolinite belong to the type II with H3 hysteresis loops, according to IUPAC-classification,[32,40] while the isotherm of PATCH-110 is intermediate between types II and IV, with an H2 hysteresis loop. The hysteresis is associated with the filling and emptying of the mesopores by capillary condensation. The particularly long and well-defined particles of PATCH, with relatively uniform lumen diameter, lead to an adsorption isotherm more characteristic of uniformly mesoporous synthetic materials. The isotherm of kaolinite shows a very minor

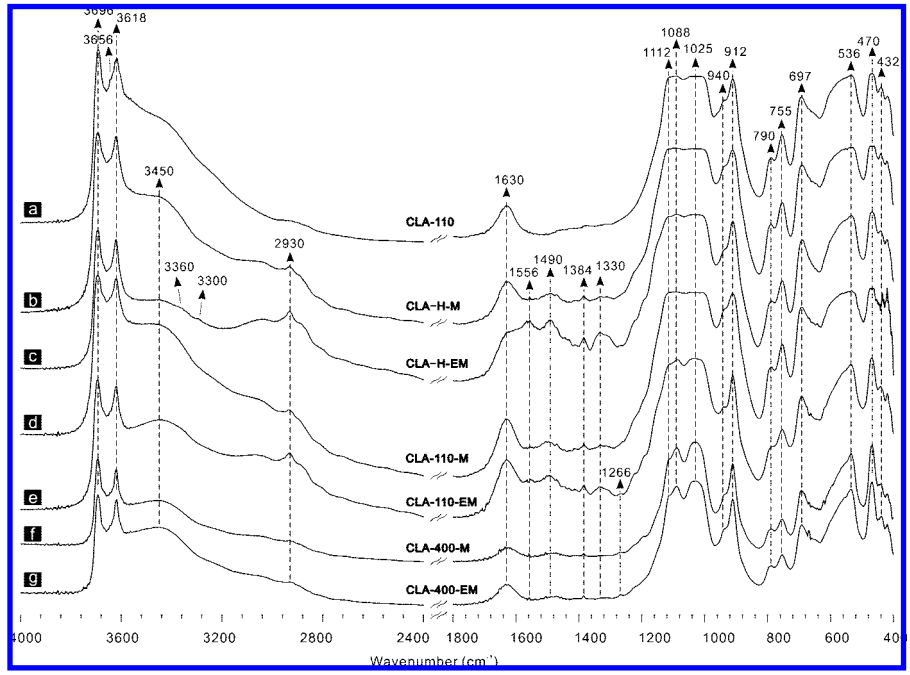

Figure 6. FTIR spectra of halloysite samples before and after modification.

TABLE 3: Positions and assignments of the IR vibration bands

position (cm^{-1})	assignments	position (cm^{-1})	assignments
3696, 3656	O−H stretching of inner-surface hydroxyl groups	1266	deformation (scissoring) of C−H_3
3618	O−H stretching of inner hydroxyl groups	1112	perpendicular Si−O stretching
3450	O−H stretching of water	1088, 1025	in-plane Si−O stretching
3360	asymmetric stretching of N−H_2	940	O−H deformation of inner - surface hydroxyl groups
3300	symmetric stretching of N−H_2	912	O−H deformation of inner hydroxyl groups
2930	symmetric stretching of C−H_2	790	symmetric stretching of Si−O
1630	O−H deformation of water	755	perpendicular Si−O stretching
1556	deformation (scissoring) of N−H_2	697	perpendicular Si−O stretching
1490	deformation (scissoring) of C−H_2	536	deformation of Al−O−Si
1384	deformation (wagging) of C−H_2	470	deformation of Si−O−Si
1330	deformation (scissoring) of Si-CH	432	Deformation of Si−O

hysteresis loop, corresponding to relatively large mesopores resulting from disordered stacking of kaolinite particles.

3.2. FTIR and Solid NMR Analysis. Figure 6 displays the FTIR spectra of CLA-series samples before and after APTES modification. The frequency and assignment of each vibrational mode observed are listed in Table 3. These assignments are based on previous reports on halloysite and APTES-grafted silica materials.[8,31,41−43] Compared to the unmodified sample CLA-110 (Figure 6a), APTES-modified samples exhibit some new FTIR peaks, such as the stretching CH_2 vibration band around 2930 cm^{-1}, the deformation CH_2 vibration at 1490 cm^{-1}, the deformation SiCH vibration at 1330 cm^{-1}, and the deformation NH_2 vibration at ca. 1556 cm^{-1}. Furthermore, the broad peak of water OH stretch, centered at 3450 cm^{-1}, was further widened in the spectra of APTES-functionalized samples, which is attributed to the overlap with the NH_2 stretching vibration signal around 3360 cm^{-1}. All of these observations show the presence of the APTES moieties in the modified clays.

Compared to the spectrum of CLA-110 (Figure 6a), the spectra of modified samples (Figure 6b - g) show a decrease in the intensity of the OH stretching band (3656 cm^{-1}) of the inner-surface AlOH groups. This indicates that the modification was accompanied by the consumption of inner-surface AlOH, that is, grafting has taken place between these groups and hydrolyzed APTES. Furthermore, the Al−O−Si deformation signal at 536 cm^{-1} is stronger in the spectra of the modified samples than that in the original sample, supporting the occurrence of grafting. From XRD characterization it is known that the inner-surface AlOH groups in the interlayer region were not available for grafting, suggesting that the vast majority of grafting occurred on the AlOH groups at the internal surface of the lumen, which are accessible by APTES.

Since the inner AlOH groups of halloysite (between the interface of the Si−O tetrahedron and the Al−O octahedron, see Figure 1) can not be reached by APTES, its vibration signal (3618 cm^{-1}) can be used as a reference for comparing the intensity of typical peaks coming from APTES (e.g., 2930 cm^{-1}), to evaluate the extent of modification of different samples. This method shows that the extent of modification follows an order of CLA-H-EM > CLA-110-EM > CLA-H-M > CLA-110-M > CLA-400-EM > CLA-400-M. Thus, the humidity of halloysite samples is an important parameter affecting the hydrolysis of APTES and the subsequent grafting reaction. For CLA-400-M and CLA-400-EM, which underwent thermal pretreatment at *ca.* 400 °C, the extent of modification appears much lower for those pretreated at lower temperatures or nonpretreated (Figure 6f, g). This result can be explained as follows. By 400 °C, the physically adsorbed water in halloysite surface had been removed, but the structural AlOH hydroxyl groups on the inner and inner-surface were not dehydroxylated until 450−600 °C.[20] As a result, it is likely that the hydrolyzed APTES bonded to the inner surface AlOH groups at the internal

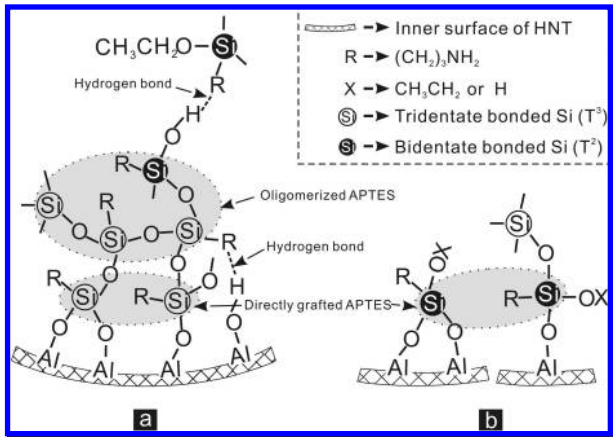

Figure 7. Schematic representation of the proposed mechanism of the formation of cross-linked network (a), and of the grafting between bidentate bonded Si and AlOH groups (b).

wall, or the AlOH or SiOH groups at the edges or external surface defects, with loss of ethanol by direct condensation of the silane silicon. This proposal is supported by the increase in intensity of the Al−O−Si peak at 536 cm^{-1}, and the Si−O−Si peak at 1088 and 1025 cm^{-1}. Because of the absence of sufficient water molecules, the APTES molecules could not hydrolyze thoroughly. The unhydrolyzed ethoxyl groups (CH_3CH_2O) are resolved in the spectra of CLA-400-M and CLA-400-EM (Figure 6f, g) by the deformation vibration signal (1266 cm^{-1}) of CH_3.

Pretreatment at 110 °C or ambient temperature did not remove physically adsorbed water thoroughly. Consequently, in addition to grafting at the internal wall, edges, and external surface, hydrolyzed APTES might also oligomerize or even polymerize with surface water, and the oligomerized APTES further reacted with grafted APTES to form a cross-linked network. The network was formed mainly through covalent bonds, but hydrogen bonding might be another way for oligomerized APTES to combine with halloysite or grafted APTES. This is supported by the existence of NH_2 vibration bands at 3360 and 3300 cm^{-1}, which have been discussed and proposed as an indication of the formation of hydrogen bonding.[41,43] The related modification mechanism is represented schematically in Figure 7a.

From the related FTIR spectra (Figure 6) it can be seen that the extent of modification for the evacuation-pretreated samples (CLA-H-EM, CLA-110-EM, and CLA-400-EM, respectively) is higher than for their nonevacuated counterparts (CLA-H-M, CLA-110-M, and CLA-400-M). These results suggest that removal of air from the lumen is useful for enhancing the loading of APTES, and hence on increasing the extent of grafting or oligomerization. This proposed mechanism explains why CLA-H-EM has the highest extent of modification, since it underwent evacuation pretreatment but did not undergo a thermal pretreatment.

Figure 8 presents the ^{29}Si CP/MAS NMR spectra of halloysite samples. The chemical shift at −92 ppm is assigned to the Q^3 silicon, $Si(OSi)_3(OAl)$, of halloysite. The signals at −68 and −61 ppm, resolved by Gauss deconvolution, are attributed to tridentate (T^3) and bidentate (T^2) bonded Si, respectively.[37] As represented diagrammatically in Figure 7a and b, the tridentate form of Si implies that all three of the ethoxyl groups of APTES were hydrolyzed and condensed with surface hydroxyl groups of halloysite or with other hydrolyzed APTES. Observation of the bidentate form of Si means that some APTES species possess one ethoxyl (or hydroxyl) group that did not hydrolyze or

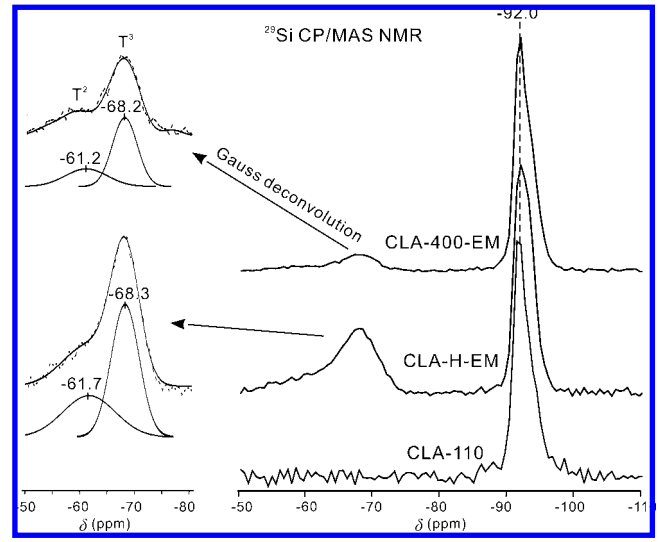

Figure 8. ^{29}Si CP/MAS NMR of APTES-modified halloysite samples. The left part shows the deconvolution results: dotted line for experimental, solid line for simulated, and separated peaks for the deconvoluted signals.

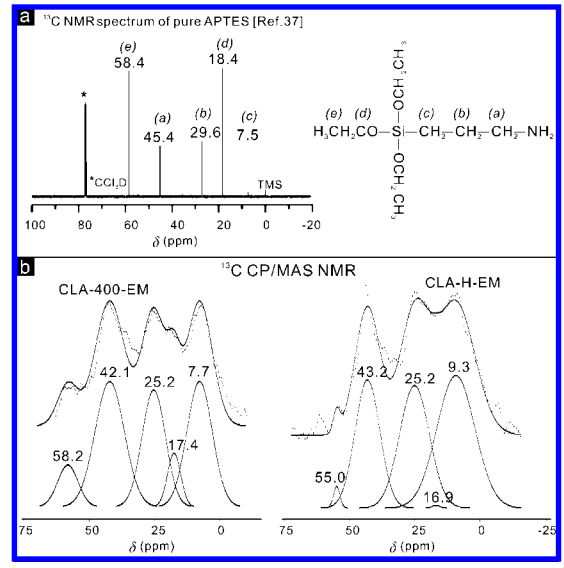

Figure 9. (a) ^{13}C NMR spectrum of pure APTES;[37] (b) ^{13}C CP/MAS NMR spectra of APTES-modified halloysite samples (dotted line for experimental, solid line for simulated, and separated peaks for the deconvolution results).

condense (Figure 7b). Based on the peak integration, the proportion of $T^3/(T^3 + T^2)$ silicon in CLA-H-EM is 63%, indicating a high extent of hydrolysis and condensation of APTES. The T^3 signal of CLA-H-EM is much stronger than that of CLA-400-EM (Figure 8a), which is in good agreement with the proposed mechanism derived from FTIR data.

Figure 9 shows the ^{13}C CP/MAS NMR spectra of CLA-H-EM and CLA-400-EM, and for comparison, the high resolution solution ^{13}C NMR spectrum of APTES recorded in $CDCl_3$.[37] In the ^{13}C CP/MAS NMR spectrum of CLA-400-EM, five signals are resolved by Gaussian deconvolution. The signals at ca. 42, 25, and 8 ppm are attributed to the carbon atoms at position (a), (b), and (c) in the propyl groups, and have an integration of 31.9, 26.8, and 27.7%, respectively. The signals at ca. 58 and 17 ppm are assigned to the carbon atoms at position (d) and (e) in ethoxyl groups,[37,43−45] and have an integration of 7.4% and 6.2%, respectively. Thus the molar ratio of ethoxyl carbon atoms over propyl carbon atoms is ca. 0.16, much lower

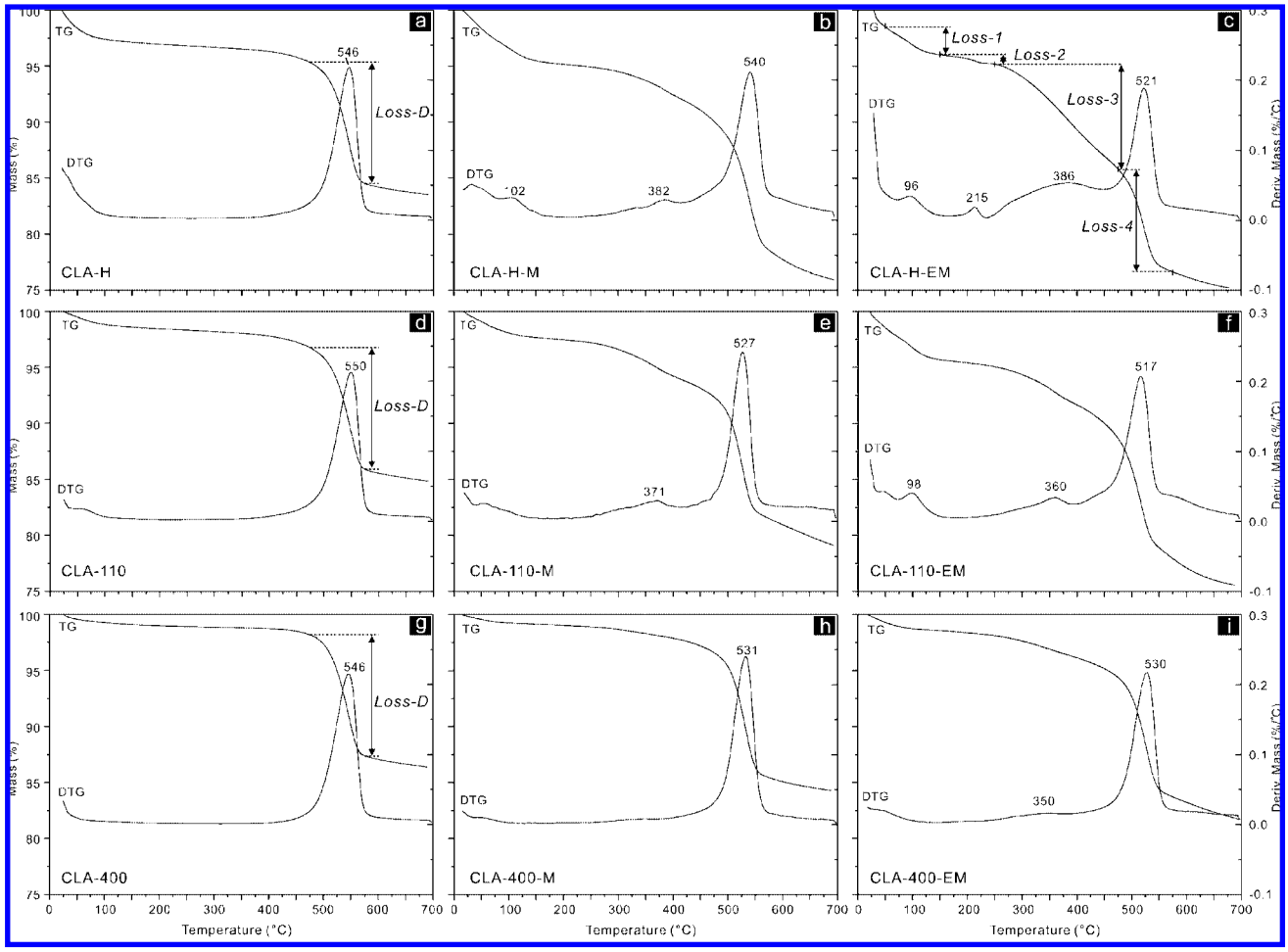

Figure 10. TG and DTG curves of original and APTES-modified halloysite samples.

than the value of 2.0 in the original APTES molecule. This result confirms that most ethoxyl groups were hydrolyzed and then consumed during the modification process. For CLA-H-EM, this ratio is only ca. 0.01, dramatically lower than for CLA-400-EM, and the related signals of ethoxyl carbon atoms at ca. 55 and 17 ppm are very weak, reflecting a high extent of hydrolysis of APTES in this sample. These results are in good agreement with the FTIR and ^{29}Si MAS NMR data.

3.3. Thermal and Elemental Analysis. Figure 10 displays the mass loss (TG) and derivative mass loss (DTG) curves of halloysite samples before and after modification. In the curves of samples that were thermally pretreated but unmodified, one major mass loss (*Loss-D*) is resolved in the temperature range of 475 − 575 °C, corresponding to the DTG peak at *ca.* 546 °C. The corresponding mass loss values for the three samples are consistent: 10.8, 10.9, and 10.8%, for samples CLA-H, CLA-110, and CLA-400 (Figure 10a, d, g). This mass loss is assigned to the dehydroxylation of structural AlOH groups of halloysite. Thermal pretreatment at 400 °C did not alter this mass loss, supporting our abovementioned proposal that at 400 °C the hydroxyl groups in the structure and on the surface had not been dehydroxylated. However, the physically adsorbed water has been substantially removed; the mass loss from 50 to 475 °C for CLA-400 (Figure 10g) is dramatically less than those for CLA-110 (Figure 10d) and CLA-H (Figure 10a).

For APTES modified samples (taking CLA-H-EM as an example, Figure 10c), four mass losses were resolved, corresponding to DTG peaks at 96, 215, 386, and 521 °C. The first mass loss (*Loss-1*) in the range 50−150 °C is due to physically adsorbed water or APTES. The mass loss (*Loss-2*) in the range 150−250 °C, corresponding to the DTG peak at 215 °C, is only well resolved in the curve of CLA-H-EM, and is attributed to hydrogen-bonded APTES existing in the cross-linking framework. The hydrogen-bonded APTES is much less thermally stable than the covalently bonded APTES, and decomposes at a lower temperature.

The third mass loss (*Loss-3*) occurring from approximately 250 to 475 °C is associated with a broad DTG peak, implying that several stages of thermal decomposition account for this mass loss. These stages include decomposition of the APTES species grafted onto SiOH and AlOH groups on edges or external surface, the oligomerized APTES, and the APTES grafted on AlOH groups at the internal surface of the lumen. The decomposition of different APTES species appears to be a slow and gradual process and overlapped partially, making a complex multistep mass loss, and thus an accurate definition on the boundary between different processes was not able to be achieved. In spite of this, the value of *Loss-M* (Table 4) in the range 50−475 °C of modified samples is shown to be a simple indication of the quantity of introduced organics, since it follows an order as CLA-H-EM > CLA-110-EM > CLA-H-M > CLA-110-M > CLA-400-EM > CLA-400-M, which is in good accordance with the FTIR results.

The fourth mass loss (*Loss-4*) over the range 475−575 °C corresponds to dehydroxylation of the residual structural AlOH groups, including the inaccessible inner AlOH groups, the inner-surface AlOH in the interlayer region, and also the unreacted AlOH groups on the inner surface of the lumen. There are two

TABLE 4: Mass Losses of Halloysite Samples Obtained from Thermal Analysis

	CLA-H-M	CLA-H-EM	CLA-110-M	CLA-110-EM	CLA-400-M	CLA-400-EM
Loss-1 (%)	2.9	2.5	1.4	2.9	0.4	0.7
Loss-2 (%)	0.6	0.8	0.5	0.6	0.2	0.7
Loss-3 (%)	4.9	9.4	4.8	6.4	2.3	3.5
Loss-4 (%)	11.5	9.2	10.9	10.7	11.2	10.7
Loss-M (%)[a]	8.3	12.7	6.7	9.9	3.0	4.9

[a] *Loss-M* = *Loss-1* + *Loss-2* + *Loss-3*.

TABLE 5: Porous Structural Data of APTES-Modified Halloysite Samples

sample	CLA-H-M	CLA-H-EM	CLA-110-M	CLA-110-EM	CLA-400-M	CLA-400-EM
S_{BET} (m^2/g)	19.7	21.3	37.0	24.7	37.0	36.0
V_{pore} (cm^3/g)	0.11	0.04	0.11	0.05	0.21	0.18

main observations arising from this part of the DTG curve. The mass loss for all of the vacuum pretreated samples is smaller than for samples modified without evacuation, indicating that fewer hydroxyl groups remain, thus confirming that evacuation promotes surface coverage and grafting. However, it is also noted that the mass loss for the samples modified without evacuation is equal or greater than the equivalent mass loss for the unmodified samples (*Loss-D*). This indicates that *Loss-4* must include some organic decomposition reactions that extend beyond 475 °C, more than making up for the small fraction of structural AlOH groups that are consumed in grafting without evacuation.

The CHN elemental analysis shows that the fractions of C and N are 6.74 and 2.20 wt % for CLA-H-EM, and 1.97% and 0.61% for CLA-400-EM. The content of loaded APTES, *M*, calculated by the fraction of N as previously described, are 19.17 and 5.32 wt %, respectively. It is noteworthy that these values are much higher than the corresponding values of *Loss-M* (Table 4), because they include the nonvolatile silicon part of APTES, which is expected to remain on the surface after thermal decomposition. Moreover, the molar ratio of C/N of CLA-H-EM and CLA-400-EM are 3.0 and 3.2, respectively, larger than the theoretical molar C/N value (2.57) of completely hydrolyzed APTES. This result indicates that incomplete hydrolysis of ethoxyl groups in APTES occurred in both of these samples,[1] and that high thermal pretreatment temperatures are correlated with a low extent of hydrolysis of APTES, which corresponds well with the spectroscopic analysis.

3.4. Porous Properties of the APTES Modified Samples. The APTES-modified halloysite samples exhibit type II nitrogen adsorption−desorption isotherms with H3 hysteresis loops (Supporting Information I), similar to that of CLA-110 (Figure 5). As anticipated, they show lower values of both specific area and porous volume in comparison with CLA-110, and these values decrease with increasing extent of modification, as shown in Table 5. To some extent the APTES-modification of halloysite is achieved at the cost of expense of porosity and specific surface area.

The pore size distributions shown in Figure 11 are calculated from the BJH method. The desorption branch of the isotherm was selected as the most appropriate for these calculations, as network-percolation effects are expected to be minor, although values will be biased toward minimum diameters and apertures.

The pore distribution for CLA-110 (Figure 11a) shows two peaks at ca. 3.4 and 11.2 nm, indicating two primary populations of pores. The ∼11 nm population can be readily identified as

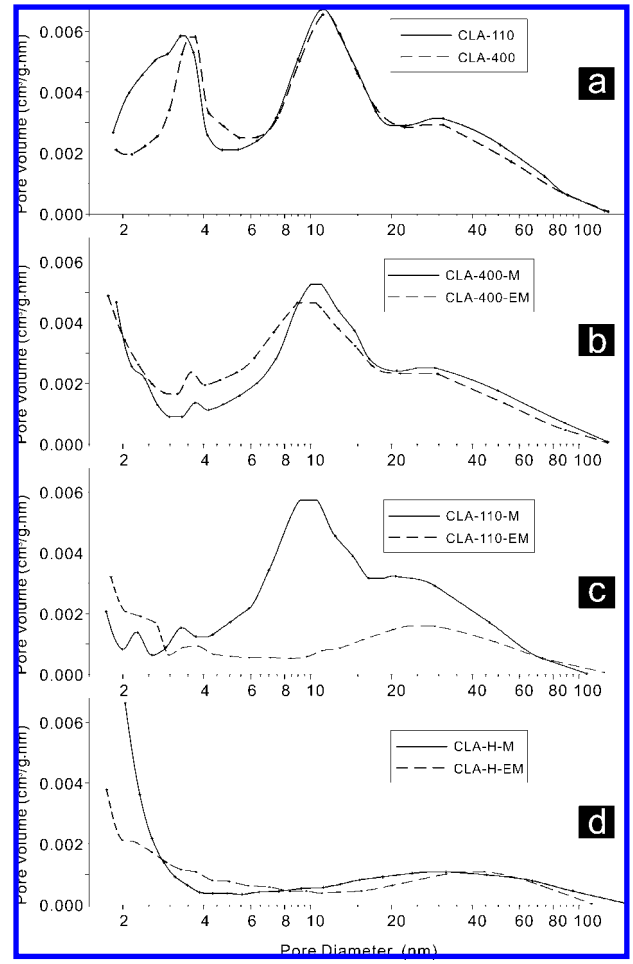

Figure 11. BJH pore size distribution curves (from desorption data) of (a) CLA-110 and CLA-400, (b) CLA-400-M and CLA-400-EM, (c) CLA-110-M and CLA-110-EM, and (d) CLA-H-M and CLA-H-EM.

the lumen of the halloysite, while the smaller pores may be spaces between particles in bundles, or lumen with partially closed openings. There is a further secondary population of pores, with diameters ranging from 15 to 50 nm. It is clear that this technique is highly complementary with TEM imaging, providing a much larger sample size, and should be recommended for evaluation of pore size of natural halloysite particles, whose pore size is generally not as uniform as synthetic mesoporous materials.

The pore distribution curves clearly show the effects of both evacuation and thermal pretreatments on the modified material. The application of evacuation pretreatment has a dramatic effect on modification of the lumen. Without evacuation (-M series) the ∼11 nm pore diameter remains largely unaffected, strongly suggesting that the air in the lumen mostly prevents penetration of APTES, although the slight narrowing of these pores in CLA-110-M (Figure 11c) may be due to the formation of a single grafted layer. The one exception is in the case of the rehydrated sample CLA-H-EM (Figure 11d), in which the abundance of physisorbed water probably allowed extensive oligomerization and polymerization, completely blocking off both ends of the lumen.

In the cases where the sample was evacuated (-EM series), the effect of modification is dependent on the pretreatment temperature. The lumen diameter of the completely dehydrated CLA-400 was reduced slightly, indicating thin layer of grafted APTES on the internal surface of CLA-400-EM (Figure 11b).

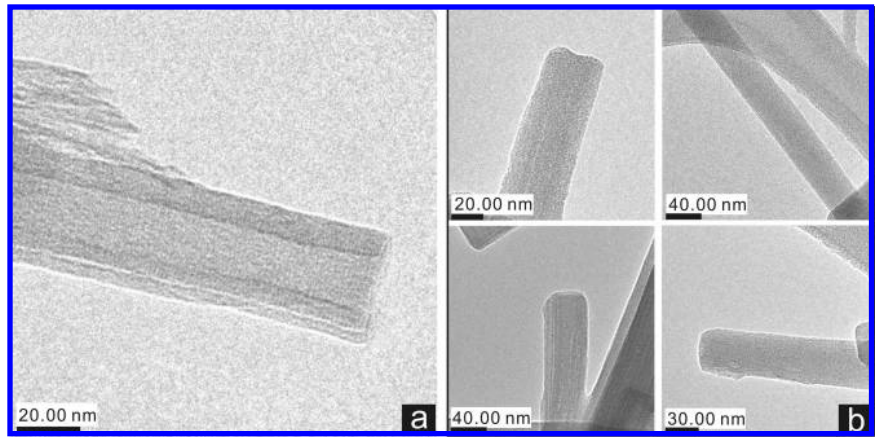

Figure 12. TEM images of (a) sample CLA, and (b) sample CLA-H-EM.

More physisorbed water was available on CLA-110 and CLA-H, promoting oligomerization and the complete blockage of the lumen (Figure 11c, d).

Finally, Figure 11 also shows that in all cases the small pore population (~3.5 nm) was largely filled with grafted or oligomerized APTES, regardless of pretreatment. The indication of microporosity in CLA-H-M is tentatively assigned to the formation of a polymerized APTES 'gel', containing small pores, due to the abundance of physisorbed water in the sample.

Adsorption measurements only characterize open porosity, and thus cannot determine whether the lumen is completely filled with APTES or is blocked only at the ends. To investigate this we used TEM imaging. As shown in Figure 12, the images of CLA-H-EM predominantly contain halloysite particles (Figure 12b) whose internal wall was less distinguished as that of CLA (Figure 12a), indicating that the lumen has been completely filled by grafted or oligomerized APTES.

3.5. Reaction Mechanism of Modification of Halloysite Nanotube with APTES. There are two mechanisms, grafting and oligomerization, for the modification of halloysite nanotubes with APTES. Grafting occurs between hydrolyzed APTES and the surface hydroxyl groups, including the aluminol groups at internal surface of lumen and the aluminol and silanol groups at edges or external surface defects. As already discussed, modification of the internal surface is relevant for immobilization and controlled release applications, while modification of the external surface and edges is beneficial for nanocomposite applications. There is little attention in the literature to the modification of the external surface of halloysite nanotubes, since the siloxane surface is generally regarded as nonreactive, except for some attempts to modify the interlayer region by intercalation.[36,46,47] Interestingly, our TEM and AFM work shows that surface defects generally exist on the external surface of halloysite nanotubes, with the hydroxyl groups at those defects potentially available for surface modification. It should be noted that an estimation of the amount of these extra external hydroxyl groups is difficult to make at this stage. In spite of this, it would be worthwhile to attempt to use the APTES modified halloysite nanotubes to prepare clay/polymer nanocomposites, as well as to evaluate the effects of external surface modification on the properties of nanocomposites.

Oligomerization occurs when there is sufficient water physically adsorbed on the surface of halloysite for complete hydrolysis of APTES. The hydrolyzed APTES species condense with previously directly grafted APTES or with each other to form a cross-linked structure. Some hydrolyzed APTES may also be bonded with the cross-linked structure by hydrogen bonds. Consequently, the occurrence and the extent of oligomerization are highly influenced by the thermal pretreatment, which determines the humidity of the halloysite sample. Heating at 400 °C showed an obvious effect on restraining the oligomerization, and in this case most of the hydrolyzed APTES connected with the halloysite surface by direct grafting. For the halloysite samples thermally pretreated at only 110 °C, and for the rehydrated samples, there was sufficient physically adsorbed water so that pronounced oligomerization occurred.

Evacuation pretreatment plays another important role for the oligomerization inside the lumen of halloysite, as this can introduce more APTES species into the lumen. For example, the nonevacuation pretreated CLA-110-M possesses a porous structure, but the pretreated sample, CLA-110-EM, exhibits a loss of most porous properties, as shown by the pore diameter distribution curves.

Consequently, pretreatment measures for modification of halloysite nanotubes need to be carefully selected in different applications. For instance, in the fields of immobilization and controlled release, where directly grafted APTES on internal surface is desirable for hosting guests, oligomerization inside the lumen needs to be restrained to allow more guests to be loaded. Thus, thermal pretreatment at 400 °C should be used. In contrast, the existence of cross-linked structure formed by oligomerized APTES might be useful for adsorption of organic pollutants, for which pretreatment at 400 °C might be unnecessary. Therefore the pretreatment conditions must be optimized for the requirements of each application.

The FTIR and TGA results and related discussions of PATCH, HG and kaolinite samples are provided in Supporting Information II and III, respectively. It was found that under the same pretreatment conditions, the organic content of CLA-110-M and PATCH-110-M was much higher than for HG-110-M. Furthermore, the extent of modification of kaolinite-110-M was much lower than for halloysite samples, with only very minor peaks assigned to APTES being resolved in the FTIR spectrum. Since the particle thickness of kaolinite is tens, or even hundreds, of times larger than the wall thickness of halloysite nanotubes, the external surface area, and thus number of available hydroxyl groups, is much less. The diversity of morphological parameters, such as particle length, external diameter and lumen diameter, between halloysite samples from different sources is expected to result in wide variations of both specific surface area and the density of available hydroxyl groups on the surface. Note that, while the density of hydroxyl groups is likely to be correlated with surface area, the ratio of external/internal diameters and the density of external surface defects

with siloxane groups will also have a large bearing. To assess whether raw halloysite samples are suitable for modification, it would be advantageous to apply detailed studies with TEM and/or AFM, nitrogen adsorption with pore size analysis, and possibly direct chemical analysis for investigation of hydroxyl density by a D_2 or D_2O isotopic exchange method.[48]

4. Conclusions

Functionalization of natural halloysite nanotubes can be achieved by modification with organosilane APTES. The mechanism of modification includes not only the direct grafting of APTES onto the surface hydroxyl groups, but also oligomerization, in which hydrolyzed APTES condenses with itself and the already grafted APTES to form a cross-linked structure. Some hydrolyzed APTES may also bridge via hydrogen bonds. For a given sample, the modification mechanism is strongly affected by the thermal and evacuation pretreatments. Thermal pretreatment affects the modification by controlling the water content. Modification of samples pretreated to 400 °C, which results in removal of the physically adsorbed water, occurred via the condensation of hydrolyzed APTES directly with hydroxyl groups at the internal wall, at the edge, and at defects of the external surface, with oligomerization greatly restrained. Without thermal pretreatment the APTES molecules hydrolyze thoroughly, and considerably more APTES is deposited on the nanotube by oligomerization. It was also found that evacuation pretreatment can dramatically enhance the loading of hydrolyzed APTES into the lumen of halloysite nanotubes.

The quantity of available hydroxyl groups, which determines the content of grafted APTES, is highly dependent on the morphological parameters (length, external and internal diameter, and wall thickness) of the halloysite nanotubes. Kaolinite is much less reactive for APTES modification than halloysite due to its very low content of available hydroxyl groups. As a whole, the modification mechanism was controlled by both the characteristics of original clay samples and the pretreatment conditions.

Halloysite is very promising for applications in the fields of nanocomposites, enzyme immobilization, and controlled release. The organosilane functionalization described is useful for improving the properties of halloysite for these applications. The results here show that the modification methods and the raw tubular halloysite sample must be tailored to meet the requirements of a specific application.

Acknowledgment. Financial support from the Australian Research Council (Grant No. LP0209078) and the Knowledge Innovation Program of the Chinese Academy of Sciences (Grant No. GIGCX-07-11/21) are gratefully acknowledged. The authors would like to thank Dr. Simon Iremonger, Dr. Greg Halder, Dr. Jarrod Amoore, Mr. Shaun Bulcock, Dr. Pall Thordarson, and Mr. Adam Sikorski, all of the University of Sydney, for their assistance in porosity measurement, thermal analysis, TEM, FM and XRD characterization.

Supporting Information Available: The N_2 adsorption−desorption isothermal curves of modified CLA-based samples and the FTIR and TG/DTG results of PATCH-, HG- and kaolinite-based samples. This material is available free of charge via the Internet at http://pubs.acs.org.

References and Notes

(1) Chong, A. S. M.; Zhao, X. S. *J. Phys. Chem. B* **2003**, *107*, 12650.
(2) Lim, M. H.; Stein, A. *Chem. Mater.* **1999**, *11*, 3285.
(3) Stein, A.; Melde, B. J.; Schroden, R. C. *Adv. Mater.* **2000**, *12*, 1403.
(4) Price, P. M.; Clark, J. H.; Macquarrie, D. J. *J. Chem. Soc., Dalton Trans.* **2000**, (2), 101.
(5) Yiu, H. H. P.; Wright, P. A. *J. Mater. Chem.* **2005**, *15*, 3690.
(6) Yuan, P.; Yang, D.; Lin, Z. Y.; He, H. P.; Wen, X. Y.; Wang, L. J.; Deng, F. *J. Non-Cryst. Solids* **2006**, *352*, 3762.
(7) Carrado, K. A. *Appl. Clay Sci.* **2000**, *17*, 1.
(8) Tonle, I. K.; Ngameni, E.; Njopwouo, D.; Carteret, C.; Walcarius, A. *Phys. Chem. Chem. Phys.* **2003**, *5*, 4951.
(9) Celis, R.; Hermosin, M. C.; Cornejo, J. *Environ. Sci. Technol.* **2000**, *34*, 4593.
(10) Wheeler, P. A.; Wang, J. Z.; Baker, J.; Mathias, L. J. *Chem. Mater.* **2005**, *17*, 3012.
(11) Herrera, N. N.; Letoffe, J. M.; Reymond, J. P.; Bourgeat-Lami, E. *J. Mater. Chem.* **2005**, *15*, 863.
(12) Carrado, K. A.; Xu, L. Q.; Csencsits, R.; Muntean, J. V. *Chem. Mater.* **2001**, *13*, 3766.
(13) Tunney, J. J.; Detellier, C. *Chem. Mater.* **1993**, *5*, 747.
(14) Tunney, J. J.; Detellier, C. *J. Mater. Chem.* **1996**, *6*, 1679.
(15) Mercier, L.; Detellier, C. *Environ. Sci. Technol.* **1995**, *29*, 1318.
(16) He, H. P.; Duchet, J.; Galy, J.; Gerard, J. F. *J. Colloid Interface Sci.* **2005**, *288*, 171.
(17) Johnson, L. M.; Pinnavaia, T. *J. Langmuir* **1991**, *7*, 2636.
(18) Churchman, G. J.; Carr, R. M. *Clays Clay Miner.* **1975**, *23*, 382.
(19) Alexander, L. T.; Faust, G. T.; Hendricks, S. B.; Insley, H.; McMurdie, H. F. *Am. Mineral.* **1943**, *28*, 1.
(20) Joussein, E.; Petit, S.; Churchman, J.; Theng, B.; Righi, D.; Delvaux, B. *Clay Miner.* **2005**, *40*, 383.
(21) Bates, T. F.; Hildebrand, F. A.; A., S. *Am. Mineral.* **1950**, *35*, 463.
(22) Singh, B. *Clays Clay Miner.* **1996**, *44*, 191.
(23) Singh, B.; Gilkes, R. J. *Clays Clay Miner.* **1992**, *40*, 212.
(24) Singh, B.; Mackinnon, I. D. R. *Clays Clay Miner.* **1996**, *44*, 825.
(25) Churchman, G. J.; Davy, T. J.; Aylmore, L. A. G.; Gilkes, R. J.; Self, P. G. *Clay Miner.* **1995**, *30*, 89.
(26) Levis, S. R.; Deasy, P. B. *Int. J. Pharm.* **2002**, *243*, 125.
(27) Levis, S. R.; Deasy, P. B. *Int. J. Pharm.* **2003**, *253*, 145.
(28) Liu, G. Y.; Kang, F. Y.; Li, B. H.; Huang, Z. H.; Chuan, X. Y. *J. Phys. Chem. Solids* **2006**, *67*, 1186.
(29) Shchukin, D. G.; Sukhorukov, G. B.; Price, R. R.; Lvov, Y. M. *Small* **2005**, *1*, 510.
(30) Yiu, H. H. P.; Botting, C. H.; Botting, N. P.; Wright, P. A. *Phys. Chem. Chem. Phys.* **2001**, *3*, 2983.
(31) Vansant, E. F.; Van Der Voort, P.; Vrancken, K. C. *Characterization and chemical modification of the silica surface*; Elsevier: New York, 1995; Vol. 93.
(32) Gregg, S. J.; Sing, K. S. W. *Adsorption, Surface Area and Porosity*, 2nd ed; Academic Press: London, 1982.
(33) Barrett, E. P.; Joyner, L. G.; Halenda, P. P. *J. Am. Chem. Soc.* **1951**, *73*, 373.
(34) Rocha, J.; Klinowski, J. *J. Magn. Reson.* **1990**, *90*, 567.
(35) Brindley, G. W. Order-disorder in the clay mineral structures. In *Crystal Structures of Clay Minerals and Their X-ray Identification*; Brindley, G. W., Brown, G., Eds.; Mineralogist Society: London, 1980; p 125.
(36) Frost, R. L.; Kristof, J. *Clays Clay Miner.* **1997**, *45*, 551.
(37) Tonle, I. K.; Diaco, T.; Ngameni, E.; Detellier, C. *Chem. Mater.* **2007**, *19*, 6629.
(38) Gardolinski, J. E. F. C.; Lagaly, G. *Clay Miner.* **2005**, *40*, 537.
(39) Gardolinski, J. E. F. C.; Lagaly, G. *Clay Miner.* **2005**, *40*, 547.
(40) Sing, K. S. W.; Williams, R. T. *Part. Part. Syst. Char.* **2004**, *21*, 71.
(41) White, L. D.; Tripp, C. P. *J. Colloid Interface Sci.* **2000**, *227*, 237.
(42) Madejova, J.; Komadel, P. *Clays Clay Miner.* **2001**, *49*, 410.
(43) Vrancken, K. C.; Vandervoort, P.; Gillisdhamers, I.; Vansant, E. F.; Grobet, P. *J. Chem. Soc., Faraday Trans.* **1992**, *88*, 3197.
(44) Chiang, C. H.; Liu, N.; Koenig, J. L. *J. Colloid Interface Sci.* **1982**, *86*, 26.
(45) Caravajal, G. S.; Leyden, D. E.; Maciel, G. E. *In Silanes, Surfaces and Interfaces*; Leyden, D. E., Ed.; Gordon and Breach Science Publishers: New York, 1985; p 283.
(46) Frost, R. L. *Clays Clay Miner.* **1995**, *43*, 191.
(47) Horvath, E.; Kristof, J.; Frost, R. L.; Redey, A.; Vagvolgyi, V.; Cseh, T. *J. Therm. Anal. Calorim.* **2003**, *71*, 707.
(48) Ding, W. P.; Meitzner, G. D.; Marler, D. O.; Iglesia, E. *J. Phys. Chem. B* **2001**, *105*, 3928.

JP805657T